

Testing semi-local chiral two-nucleon interaction in selected electroweak processes

R. Skibiński, J. Golak, K. Topolnicki, and H. Witała

*M. Smoluchowski Institute of Physics,
Jagiellonian University, PL-30059 Kraków, Poland*

E. Epelbaum and H. Krebs

*Institut für Theoretische Physik II,
Ruhr-Universität Bochum, D-44780 Bochum, Germany*

H. Kamada

*Department of Physics, Faculty of Engineering,
Kyushu Institute of Technology, Kitakyushu 804-8550, Japan*

Ulf-G. Meißner

*Helmholtz-Institut für Strahlen- und Kernphysik and Bethe Center for Theoretical Physics,
Universität Bonn, D-53115 Bonn, Germany*

*Institut für Kernphysik, Institute for Advanced
Simulation and Jülich Center for Hadron Physics,
Forschungszentrum Jülich, D-52425 Jülich, Germany and*

*JARA - High Performance Computing,
Forschungszentrum Jülich, D-52425 Jülich, Germany*

A. Nogga

*Institut für Kernphysik, Institute for Advanced
Simulation and Jülich Center for Hadron Physics,
Forschungszentrum Jülich, D-52425 Jülich, Germany and*

*JARA - High Performance Computing,
Forschungszentrum Jülich, D-52425 Jülich, Germany*

(Dated: March 7, 2022)

Abstract

The recently developed semi-local improved chiral nucleon-nucleon interaction is used for the first time to study several electromagnetic and weak processes at energies below the pion production threshold. Cross sections and selected polarization observables for deuteron photodisintegration, nucleon-deuteron radiative capture, three-body ${}^3\text{He}$ photodisintegration as well as capture rates for decays of the muonic ${}^2\text{H}$ and ${}^3\text{He}$ atoms are calculated. The Lippmann-Schwinger and Faddeev equations in momentum space are solved to obtain nuclear states. The electromagnetic current operator is taken as a single nucleon current supplemented by many-body contributions induced via the Siegert theorem. For muon capture processes the nonrelativistic weak current together with the dominant relativistic corrections is used. Our results compare well with experimental data, demonstrating the same quality as is observed for the semi-phenomenological AV18 potential. Compared to the older version of the chiral potential with a nonlocal regularization, a much smaller cut-off dependence is found for the state-of-art chiral local interaction employed in this paper. Finally, estimates of errors due to the truncation of the chiral expansion are given.

PACS numbers: 21.45.-v, 25.10.+s, 21.30.Fe

I. INTRODUCTION

Studies of electromagnetic and weak reactions are an important part of nuclear physics. They deliver information on electromagnetic properties of nuclei, transitions between nuclear states and details of electromagnetic and weak currents inside nuclei [1–4]. In the broader sense the precise description of electromagnetic and weak reactions is a challenging test for models of the nuclear Hamiltonian and current operators as well as for the used theoretical schemes and numerical methods. Chiral Effective Field Theory (χ EFT) is currently the most important theoretical approach, which can and should be tested in investigations of electromagnetic and weak processes. Among many attempts to do that in the few-nucleon sector we mention [2, 5, 6] and references therein. However, these works were usually restricted to small energies or the lowest orders of the chiral expansion or combine the phenomenological potentials and chiral currents within the so-called "hybrid" χ EFT approach or cover only selected reaction channels.

The continuous progress in the field of χ EFT has resulted in the development of sophisticated nucleon-nucleon (NN) and many-nucleon interactions [7, 8]. These forces have been used to describe reactions in three-nucleon (3N) systems [9–14], the structure of light nuclei [15] and nuclear matter [16]. Results obtained for NN scattering at energies up to 300 MeV and nucleon-deuteron elastic scattering proved the usefulness and high quality of chiral potentials. In these first studies the regularization of NN and 3N potentials in momentum space with the nonlocal regulator was used [17].

Recently it was shown [18, 19] that such a regularization scheme introduces artifacts and affects the correct physical behavior of the potential at long distances. In addition, the spectral function regularization had to be introduced in order to cut off the unwanted short-range part of the two-pion exchange potential. This in turn causes too strong dependence of predictions on values of the cut-off parameters [18, 20]. The Bochum-Bonn group proposed recently in Refs. [21, 22] an improved version of the chiral potential up to fifth order of the chiral expansion (N^4 LO). During its construction, regularization is performed in coordinate space and only afterwards such a regularized force is transformed to momentum space. In particular, the one-pion and the static two-pion exchange potentials are regularized in coordinate space by multiplying them by the function $f(\frac{r}{R}) = [1 - \exp(-(\frac{r}{R})^2)]^6$, with R being the cut-off (regularization) parameter. This procedure maintains the long-range part of the interaction and leads to smaller undesirable regularization effects. Indeed, as shown in [21, 22] the NN phase shifts as well as the deuteron properties are much less sensitive to the values of the regularization parameter R than the ones obtained within the older version [17]. The same is also true for elastic nucleon-deuteron (Nd) scattering observables [23]. The three-nucleon force with consistent local regularization is under development, so in this paper we only use two-body interactions and, in addition, we neglect the Coulomb force.

One of important and unique features of the χ EFT approach is a possibility of a consistent derivation of nuclear forces and electroweak current operators, see e.g. Refs. [24–28] for works in these direction. In particular, in Ref. [27] the long-range part of the leading two-pion exchange contributions was derived. Together with the well known single nucleon current (SNC) and consistent old, nonlocal version of chiral interaction they were used to study the deuteron and the ^3He photodisintegration in Refs. [29, 30]. While the general description of observables was reasonable, a strong cut-off dependence of predictions was also observed. Similar results were obtained for radiative nucleon-deuteron capture and ^3He photodisintegration where instead of explicit many-body currents the Siegert theorem was

used [31]. The strong variation of predictions due to different values of the cut-off parameters practically precluded us from drawing detailed physical conclusions. Thus it is very interesting to see whether the cut-off dependence also becomes smaller for the electromagnetic processes, when the newly developed improved chiral interactions are considered. In the present work we use the Siegert approach and postpone studies based on explicit single nucleon and many-body electromagnetic currents until a more complete picture of the electroweak current operator, consistent with the NN interaction at each order of the chiral expansion, is known.

The question of the cut-off dependence can be also addressed in weak reactions. Thus we use the improved NN forces [21, 22] to calculate the capture rates in muon capture reactions on the deuteron and ^3He . In this paper we employ a nonrelativistic single nucleon weak current operator supplemented with leading relativistic corrections (RC) [5, 32, 33]. Since we are mainly interested in the cut-off dependence of capture rates, the use of such an incomplete model of the current operator is justified in the present investigation.

The paper is organized as follows. In the next section we give a short overview of our formalism for electromagnetic and weak processes. Section III contains selected results for the deuteron photodisintegration process, $\gamma + d \rightarrow p + n$, while in Sections IV and V we discuss 3N electromagnetic processes: nucleon-deuteron radiative capture, $n(p) + d \rightarrow \gamma + ^3\text{H}(^3\text{He})$, and the total ^3He photodisintegration $\gamma + ^3\text{He} \rightarrow p + p + n$, respectively. The results for weak muon capture processes, $\mu^- + ^2\text{H} \rightarrow n + n + \nu_\mu$, $\mu^- + ^3\text{He} \rightarrow ^3\text{H} + \nu_\mu$, $\mu^- + ^3\text{He} \rightarrow n + d + \nu_\mu$ and $\mu^- + ^3\text{He} \rightarrow n + n + p + \nu_\mu$ are presented in Section VI. We summarize in Section VII.

II. FORMALISM

The theoretical approach used in the present study is described in detail in [29, 34–37], so here we only remind the reader of the key steps. We work in momentum space and employ a formalism based on the 3N Faddeev equations. The nuclear matrix elements for electromagnetic or weak disintegration processes are the central quantities from which we are able to calculate observables [33, 36].

In the case of the deuteron photodisintegration, the nuclear matrix element N_{deu}^μ is defined as

$$N_{deu}^\mu \equiv \langle \Psi_{\text{scatt}}^{2N} | j_{2N}^\mu | \Psi_{\text{bound}}^{2N} \rangle, \quad (2.1)$$

where $|\Psi_{\text{scatt}}^{2N}\rangle$ and $|\Psi_{\text{bound}}^{2N}\rangle$ are the final proton-neutron scattering state and the initial deuteron bound state, respectively. The deuteron state is a solution of the Schrödinger equation with the Hamiltonian comprising the NN potential V . The same interaction, together with the free two-nucleon (2N) propagator G_0 , enters the Lippmann-Schwinger equation for the t operator, $t = V + tG_0V$, which we use to obtain the final scattering state. Then the N_{deu}^μ is given as

$$N_{deu}^\mu = \langle \vec{p}_0 | (1 + tG_0) j_{2N}^\mu | \Psi_{\text{bound}}^{2N} \rangle, \quad (2.2)$$

where $|\vec{p}_0\rangle$ is the eigenstate of the relative proton-neutron momentum. The form of the electromagnetic current operator j_{2N}^μ is discussed below.

Radiative nucleon-deuteron capture is related via the time reversal symmetry to the two-body ^3He or ^3H photodisintegration reactions. We exploit this relation and calculate the nuclear matrix element for the radiative Nd capture N_{radNd}^μ from the matrix element $N_{Nd}^\mu \equiv \langle \Psi_{\text{scatt}}^{Nd} | (1 + P)j_{3N}^\mu | \Psi_{\text{bound}}^{3N} \rangle$ for the photodisintegration reaction, leading to the

final nucleon-deuteron scattering state $|\Psi_{\text{scatt}}^{Nd}\rangle$ [34, 36]. The matrix element N_{Nd}^μ can be expressed as

$$N_{Nd}^\mu = \langle \phi_{Nd} | (1 + P) j_{3N}^\mu | \Psi_{\text{bound}}^{3N} \rangle + \langle \phi_{Nd} | P | U^\mu \rangle, \quad (2.3)$$

where $|\Psi_{\text{bound}}^{3N}\rangle$ is the 3N bound state while $|\phi_{Nd}\rangle$ is the product of the internal deuteron state and the state describing the free relative motion of the third nucleon with respect to the deuteron. $P = P_{12}P_{23} + P_{13}P_{23}$ is a permutation operator with P_{ij} being the operator exchanging nucleons i and j .

The auxiliary state $|U^\mu\rangle$ fulfills the Faddeev-like equation [36]

$$|U^\mu\rangle = tG_0(1 + P)j_{3N}^\mu|\Psi_{\text{bound}}^{3N}\rangle + tG_0P|U^\mu\rangle, \quad (2.4)$$

with the free 3N propagator G_0 .

The nuclear matrix element for ^3He photodisintegration leading to three free nucleons in the final state, $N_{3N}^\mu \equiv \langle \Psi_{\text{scatt}}^{3N} | j_{3N}^\mu | \Psi_{\text{bound}}^{3N} \rangle$, is also given by the auxiliary state $|U^\mu\rangle$:

$$N_{3N}^\mu = \langle \Phi_{3N} | (1 + P) j_{3N}^\mu | \Psi_{\text{bound}}^{3N} \rangle + \langle \Phi_{3N} | (1 + P) | U^\mu \rangle, \quad (2.5)$$

where $|\Phi_{3N}\rangle$ is an antisymmetrized state describing the free motion of the three outgoing nucleons.

The nuclear electromagnetic current operators, j_{2N}^μ and j_{3N}^μ , employed for the deuteron and ^3He (^3H) photodisintegration processes, are constructed in the same way. Unfortunately the 2N currents fully consistent with the locally regularized nuclear potentials are not yet available. Therefore, we approximate the electromagnetic current by a sum of contributions from the individual nucleons and supplement these results by the many-body parts incorporated via the Siegert theorem [34, 36]. To this end we perform a multipole decomposition of the corresponding single nucleon current matrix elements and use standard identities [36] to express a part of the electric multipoles by the Coulomb multipoles, generated again by the single nucleon charge density operator. This step is justified by the fact that at low energies many-nucleon contributions to the nuclear charge density are small. The remaining part of the electric multipoles and all the magnetic multipoles are taken solely from the single nucleon current operators. The Siegert theorem, together with the so-called Siegert hypothesis, is also widely used in many calculations performed in coordinate space, see e.g. [1, 38–40]. This form of the nuclear current operator has the (purely technical) advantage that it does not depend on the nucleon-nucleon potential employed in our calculations. We denote this model of the current operator as SNC+Siegert.

The weak muon capture processes on atomic nuclei are described by means of similar nuclear matrix elements as in Eqs. (2.1)-(2.5), which are combined with the well-known leptonic part [41], to build the full transition amplitudes. Depending on the studied process the deuteron or ^3He wave function represents the initial nuclear bound state. For the $\mu^- + ^2\text{H} \rightarrow \text{n} + \text{n} + \nu_\mu$ reaction, the final two-neutron scattering state is calculated using the t -operator. In the case of break-up channels in muon capture on ^3He the corresponding two- and three-body scattering states are required. We calculate them analogously to the states for photodisintegration, again using Eq.(2.4), with the electromagnetic current j_{3N}^μ replaced by the weak current j_w^μ [5, 32, 33]. Since we solve Eq.(2.4) at a given energy of the 3N system, numerous solutions of Faddeev-like equation (2.4) have to be obtained in order to cover the whole range of the final muon neutrino energies. This significantly increases the numerical complexity of such calculations. Of course, in the case of $\mu^- + ^3\text{He} \rightarrow ^3\text{H} + \nu_\mu$ channel we use only pre-calculated ^3He and ^3H states and no Faddeev equation for the bound state has

to be solved repeatedly. For the weak current j_w^μ we employ a non-relativistic single nucleon current operator supplemented by the dominant $(p/M_{nucl})^2$ relativistic corrections, where M_{nucl} is the nucleon mass. A detailed discussion of the weak current, formulas connecting the nuclear matrix elements with the capture rates and various aspects of the reaction kinematics are given in [33].

Our calculations are performed in momentum space and we use the formalism of partial waves. In the calculations we employ all partial waves in the two-body systems up to the two-body total angular momentum $j \leq 3$ and in the three-body states up to the three-body total angular momentum $J \leq \frac{15}{2}$. Such sets of partial waves guarantee convergence of predictions for all observables, see [36, 42] for more technical details. The 3N bound states are obtained as in Ref. [43].

To estimate the theoretical errors of predictions arising from neglecting, at a given order of the chiral expansion, the contributions from higher orders, we apply the prescription given in [23, 44]. Namely, we estimate the truncation error $\delta(X)^{(i)}$ of an observable X at i -th order of the chiral expansion, with $i = 0, 2, 3, \dots$. If Q denotes the chiral expansion parameter, the expressions for truncation errors are

$$\begin{aligned}\delta(X)^{(0)} &\geq \max(Q^2|X^{(0)}|, |X^{(i \geq 0)} - X^{(j \geq 0)}|), \\ \delta(X)^{(2)} &= \max(Q^3|X^{(0)}|, Q|\Delta X^{(2)}|, |X^{(i \geq 2)} - X^{(j \geq 2)}|), \\ \delta(X)^{(i)} &= \max(Q^{i+1}|X^{(0)}|, Q^{i-1}|\Delta X^{(2)}|, Q^{i-2}|\Delta X^{(3)}|) \text{ for } i \geq 3.\end{aligned}\quad (2.6)$$

In the above formulas $X^{(i)}$ is a prediction for the observable X at i -th order, $\Delta X^{(2)} \equiv X^{(2)} - X^{(0)}$ and $\Delta X^{(i)} \equiv X^{(i)} - X^{(i-1)}$ for $i \geq 3$. We also require that $\delta(X)^{(2)} \geq Q\delta(X)^{(0)}$ and $\delta(X)^{(i)} \geq Q\delta(X)^{(i-1)}$ for $i \geq 3$. In particular, such a way of theoretical error estimation takes into account the fact that our present calculations are incomplete as we do not include the 3N force starting from N²LO. Furthermore, we do *not* estimate in this paper the uncertainty from the truncation of the chiral expansion of the current operators, which are included by means of the Siegert theorem at all considered orders. The actual theoretical uncertainty may, therefore, be larger than the values of $\delta(X)^{(i)}$ given below. A more reliable uncertainty quantification requires performing complete calculations including the corresponding 3N forces and exchange current operators. This work is in progress.

III. RESULTS FOR DEUTERON PHOTODISINTEGRATION

In Fig. 1 we show the total cross section for $\gamma + d \rightarrow n + p$ process at photon laboratory energies E_γ up to 80 MeV obtained using the chiral NN interaction at N⁴LO [21, 22] with the value of the regularization parameter $R=0.9$ fm. In this case we apply two models of the electromagnetic current: the SNC alone (the dashed red curve) and the SNC+Siegert (the thick dashed black curve). It is clear that while the omission of 2N currents leads to a poor description of the data, the SNC+Siegert approach yields an excellent agreement with the experimental results. For the sake of comparison with the predictions based on semi-phenomenological forces, we show also predictions obtained with the AV18 NN interaction [45] and three models of the nuclear current: SNC (green double-dotted-dashed curve), SNC+Siegert (dotted violet curve) and SNC+MEC (blue solid curve). The SNC+MEC model comprises single nucleon contributions and the explicit π -like and ρ -like meson exchange currents (MEC) linked to AV18 NN interaction (see [34, 36] for more details). We observe that for this observable the implicit (SNC+Siegert) and explicit (SNC+MEC) ways

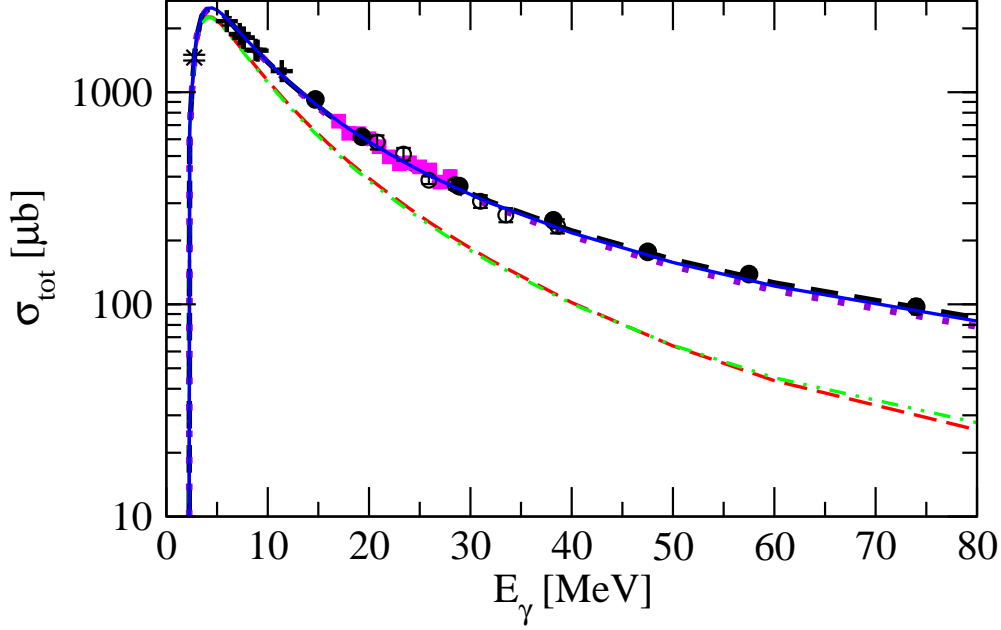


FIG. 1. (Color online) The total cross section σ_{tot} for the $\gamma + d \rightarrow p + n$ reaction. The chiral $N^4\text{LO}$, $R=0.9$ fm predictions for the SNC (SNC+Siegert) current model are shown with the dashed red (thick black dashed) curve. The AV18 predictions for the SNC, SNC+Siegert and SNC+MEC current models are shown with the double-dotted-dashed green, dotted violet and solid blue curve, respectively. The experimental data are from Ref. [46] (black "x"), [47] (magenta squares), [48] (open circles), [49] (black pluses) and [50] (black dots).

of including many-body contributions to the current operator give quite similar predictions, which are in a very good agreement with the data, when the AV18 NN potential is used to generate the 2N states. Further, the SNC+Siegert approach to the current operator works equally well with the chosen chiral and the AV18 NN potentials. In both cases we obtain very similar predictions, practically indistinguishable at photon energies below approximately 30 MeV. At the higher energies a small difference develops between the chiral and the AV18 potential, with the chiral predictions lying closer to the data.

Next we study a more detailed observable, namely the differential cross section at two photon laboratory energies $E_\gamma=30$ MeV (Fig. 2, the upper row) and $E_\gamma=100$ MeV (Fig. 2, the lower row). In the left panel we show the convergence of predictions for $R=0.9$ fm with respect to the order of the chiral expansion. In the middle panel the uncertainty of theoretical predictions due to the truncation of higher order contributions is given. Finally, in the right panel, we demonstrate the dependence of predictions on the values of the regulator R at $N^4\text{LO}$ using five different values of R : 0.8, 0.9, 1.0, 1.1 and 1.2 fm. Our best prediction, SNC+Siegert for $R=0.9$ fm is represented by the thick black dashed curve and is shown both in the left and right panels. For the sake of comparison, also the AV18 prediction given by the thick violet dotted line is displayed in these two panels. The same arrangement of curves will be preserved also in Figs. 3-6, 8 and 12.

It is clear that for both energies one has to go beyond the leading order (LO) to describe data. At the lower energy all the higher than LO predictions are close to each other, but at $E_\gamma=100$ MeV the convergence is reached only at $N^3\text{LO}$. The truncation errors presented in the central panel confirm this observation and the band at $N^4\text{LO}$ lies on the $N^3\text{LO}$

one. A small but visible width of the $N^4\text{LO}$ band for the higher energy suggests that some contributions from higher orders are still possible for this observable. The cut-off dependence of the cross section is very small at lower energy and increases with energy, reaching at $E_\gamma=100$ MeV about 20% at small proton c.m. scattering angles. However, a more careful analysis reveals that predictions obtained with $R=1.1$ fm and $R=1.2$ fm are clearly far from the other ones, which are closer to each other. This observation is in agreement with the behaviour of the cross section for the NN and Nd elastic scattering [23, 44] and provide yet another indication that the theoretical uncertainty of the calculations using $R=1.1$ fm and $R=1.2$ fm is dominated by finite-regulator artifacts, see Ref. [21] for more details. Importantly, the cut-off dependence of the cross section observed here for the semi-local chiral force is much smaller than the cut-off dependence observed for the older version of the potential with the nonlocal regularization. As shown in Fig. 1 of Ref. [29] (pink band) for the older potential the cut-off dependence reaches 25% already at $E_\gamma=30$ MeV and increases with photon energy. For the improved chiral force at $N^4\text{LO}$ all predictions are slightly above the cross section calculated with the AV18 potential. The data at $E_\gamma=100$ MeV and at small angles between proton and photon momenta are better described by the AV18 force while data at bigger angles are closer to the chiral predictions.

We choose the deuteron tensor analyzing powers T_{20} and T_{22} as examples of polarization observables. Such observables are supposed to be more sensitive to the NN interaction and the current operator used in the calculations. A measurement of these observables at proton scattering angle $\theta_p^{c.m.} = 88^\circ$ has been reported in Ref. [52]. In Fig. 3 we compare our predictions for T_{20} (top) and T_{22} (bottom) with precise data from Ref. [52] and with older data from Ref. [53] for photon laboratory energies below $E_\gamma=140$ MeV. The analyzing power T_{20} is very well described by chiral predictions but for T_{22} a clear discrepancy is seen with both sets of data above $E_\gamma=50$ MeV. The predictions based on the chiral semi-local force show, for both analyzing powers, similar behaviour as for the differential unpolarized cross section - their convergence with respect to the chiral expansion, truncation errors and cut-off dependence are very reasonable. Even for the highest energies the difference between $N^3\text{LO}$ and $N^4\text{LO}$ predictions is below 1.6% (1.3%) and the difference between predictions based on different values of the R parameter does not exceed 7.3% (3.1%) for T_{20} (T_{22}). Note that if we omit predictions with $R=1.2$ fm, the latter numbers change to 2.3% (1.4%). The size of the truncation errors shows that only small contribution from higher orders can be expected even at energies above $E_\gamma=50$ MeV.

It has been shown by Arenhövel and collaborators [52, 54] in calculations with semi-phenomenological NN forces that a more complete 2N current operator including in addition to the implicit MEC (incorporated in the Siegert approach) also other explicit 2N operators, isobar configurations and leading order relativistic corrections leads to a much better description of T_{22} . Thus, the poor description of T_{22} data in Fig. 3 can be attributed to the weaknesses of our model for the 2N electromagnetic current. This is interesting in view of future studies which will be performed with NN interactions and current operators consistently derived within the χEFT framework. We would like to stress that such studies would benefit from precise measurements of the deuteron analyzing powers at energies below $E_\gamma=140$ MeV in the whole range of scattering angles.

For the deuteron photodisintegration reaction also data for the photon asymmetry are available. In a recent precision experiment [55] the photon asymmetry Σ_γ has been measured at the proton c.m. scattering angle $\theta = 90^\circ$, for the low photon laboratory energies up to 4.05 MeV. In Fig. 4 we compare our results with these data. As can be expected at such

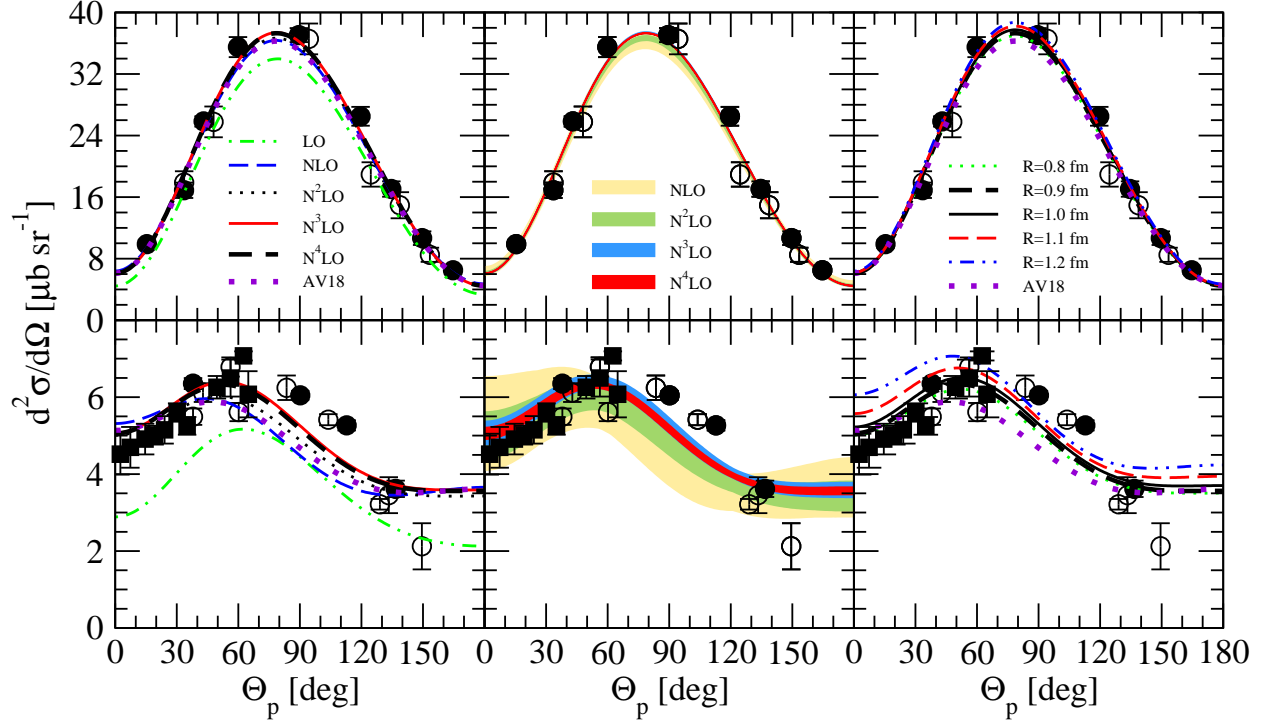


FIG. 2. (Color online) The differential cross section $\frac{d^2\sigma}{d\Omega}$ for the $\gamma + d \rightarrow p + n$ reaction at $E_\gamma=30$ MeV (the upper row) and $E_\gamma=100$ MeV (the lower row) as a function of the proton c.m. scattering angle θ_p . The left column shows the convergence of predictions at $R=0.9$ fm with respect to the order of the chiral expansion (the double-dotted-dashed green, dashed blue, dotted black, solid red and thick dashed black curves correspond to predictions at LO, NLO, N^2 LO, N^3 LO and N^4 LO, respectively). The middle column shows the truncation errors (see text) at the different orders of the chiral expansion: NLO (yellow band), N^2 LO (green band), N^3 LO (turquoise band) and N^4 LO (red band). The right column shows the dependence of predictions at N^4 LO on the value of parameter R (the dotted green, thick dashed black, solid black, dashed red and double-dotted-dashed blue curves correspond to predictions with $R=0.8, 0.9, 1.0, 1.1$ and 1.2 fm, respectively). Note that the thick dashed black curve shown in both margin columns represents the same predictions. Also the thick violet dotted curve which represents the AV18 predictions is duplicated in the margin columns. All data points (open and solid circles and full squares) are from [51].

low energies even predictions at lower orders are sufficient to describe the data. The results at N^2 LO, N^3 LO and N^4 LO practically overlap. Also the predictions for different values of the R regulator are very close to each other. The agreement with the data is excellent.

A precise measurement of the photon asymmetry in the $\gamma + d \rightarrow p + n$ reaction as a function of the neutron c.m. scattering angle at several photon energies has been reported in [56]. We choose two of them: $E_\gamma=19.8$ MeV and 60.8 MeV to give examples for small and medium photon energies. In Fig. 5 we compare our results with the data from [56] and [57, 58]. At the lower photon energy we observe a similar picture as for the photon

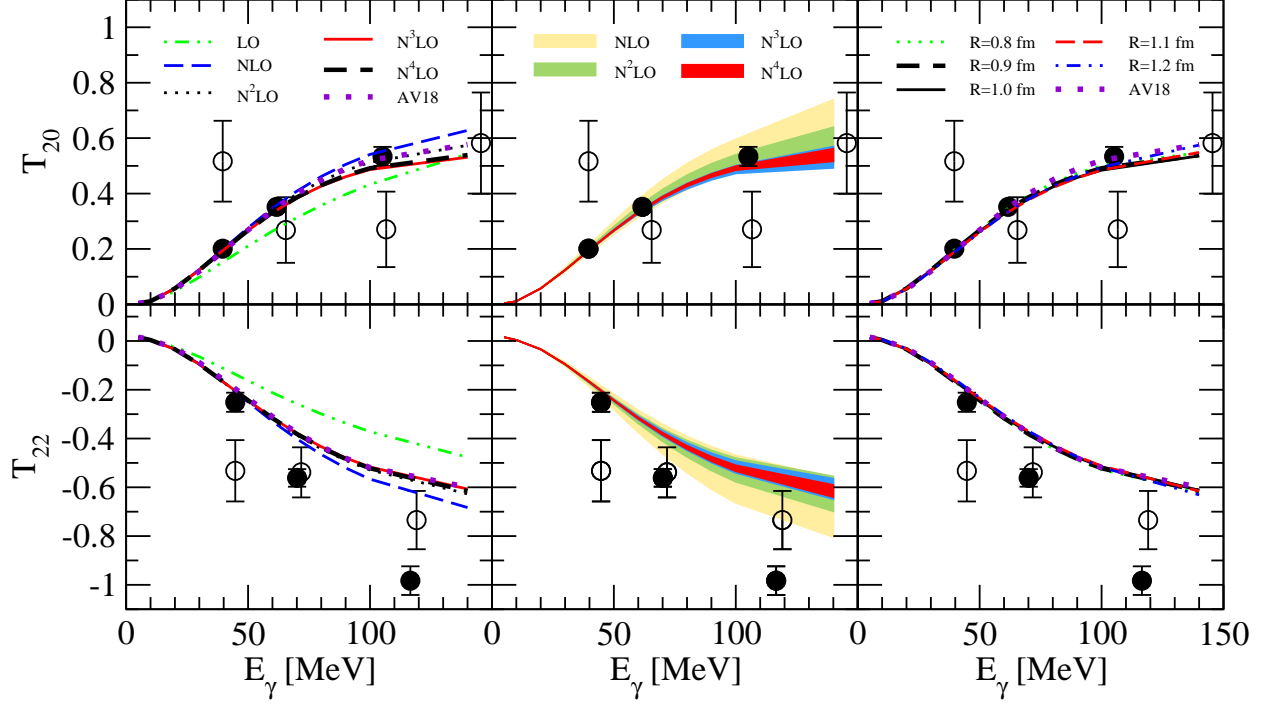


FIG. 3. (Color online) The deuteron analyzing powers T_{20} (top) and T_{22} (bottom) for the $\gamma + d \rightarrow p + n$ reaction at $\Theta_p^{c.m.} = 88^\circ$ and for E_γ up to 150 MeV. The left column shows the convergence of predictions at $R=0.9$ fm with respect to the order of the chiral expansion (curves as in Fig. 2). The middle column shows the truncation errors (see text) at different orders of the chiral expansion (bands as in Fig. 2). The right column shows the dependence of predictions at $N^4\text{LO}$ on the value of the R parameter (curves as in Fig. 2). The data are from [52] (filled circles) and [53] (open circles).

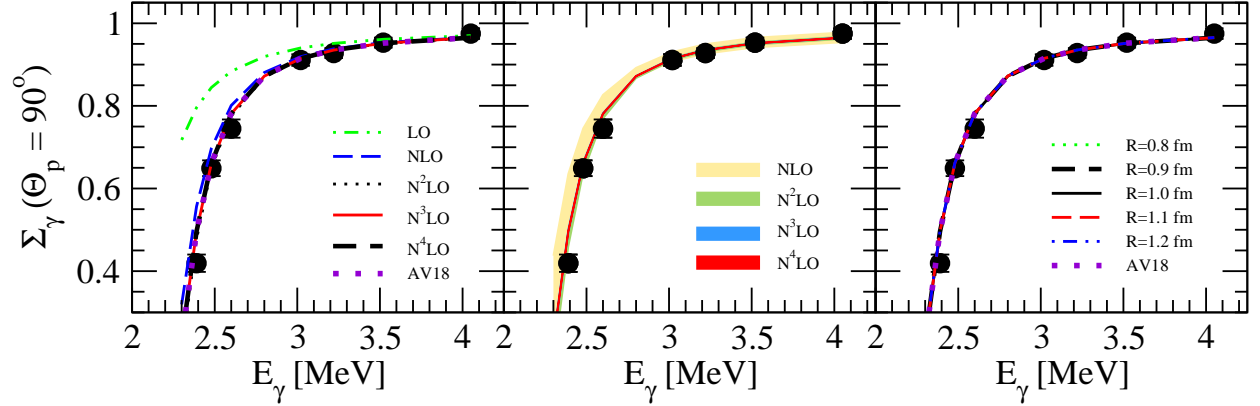


FIG. 4. (Color online) The photon asymmetry $\Sigma_\gamma(\theta_p = 90^\circ)$ at proton c.m. scattering angle $\theta_p = 90^\circ$ for the $\gamma + d \rightarrow p + n$ reaction at low photon energies. The left column shows the convergence of predictions at $R=0.9$ fm with respect to the order of the chiral expansion (curves as in Fig. 2). The middle column shows the truncation errors (see text) at the different orders of the chiral expansion (bands as in Fig. 2). The right column shows the dependence of predictions at $N^4\text{LO}$ on the value of the R parameter (curves as in Fig. 2). The data are from [55].

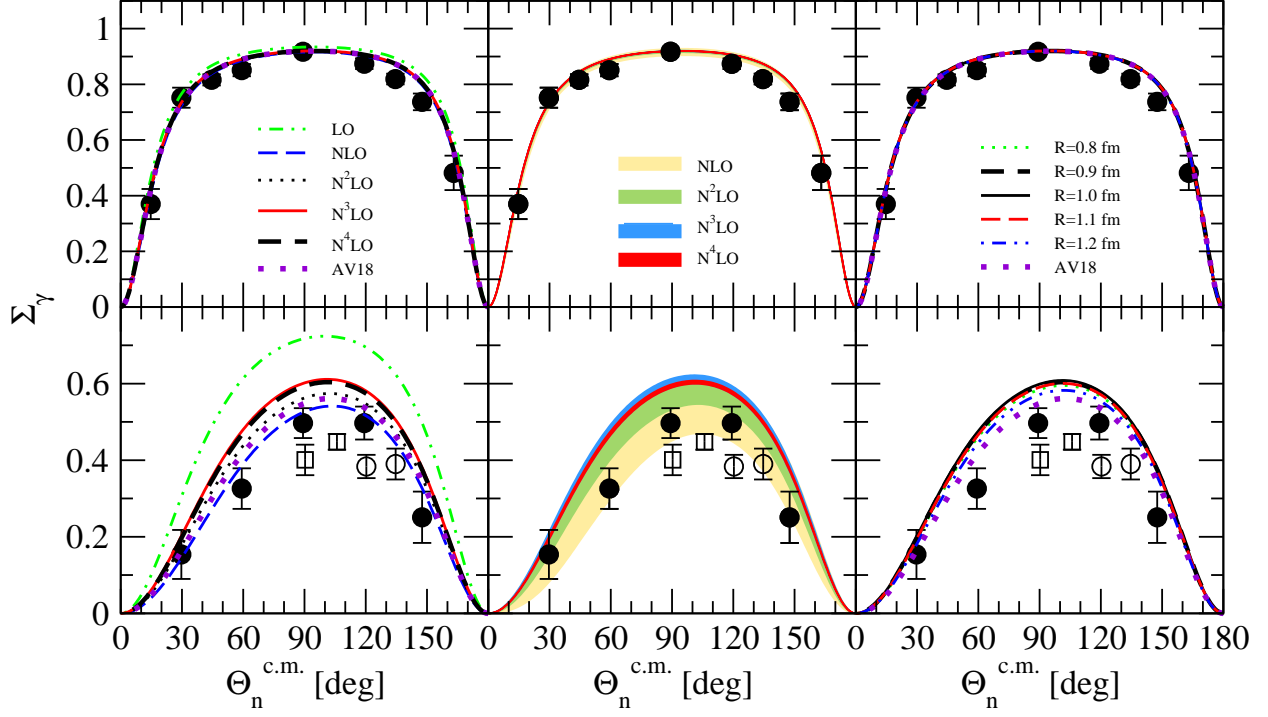


FIG. 5. (Color online) The photon asymmetry Σ_γ for the $\gamma + d \rightarrow p + n$ reaction at $E_\gamma=19.8$ MeV (top) and 60.8 MeV (bottom) as a function of neutron c.m. scattering angle $\theta_n^{c.m.}$. The left column shows the convergence of predictions at $R=0.9$ fm with respect to the order of the chiral expansion (curves as in Fig. 2). The middle column shows the truncation errors (see text) at the different orders of the chiral expansion (bands as in Fig. 2). The right column shows the dependence of predictions at $N^4\text{LO}$ on the value of the R parameter (curves as in Fig. 2). The data are from [56] (filled circles), [57] (empty circles) and [58] (squares).

asymmetry $\Sigma_\gamma(\theta_p = 90^\circ)$: predictions are insensitive to the regulator value and to the order of the NN interaction. Even predictions at LO describe data at $E_\gamma=19.8$ MeV reasonably well. At $E_\gamma=60.8$ MeV predictions for the photon asymmetry become convergent only at $N^3\text{LO}$. The truncation errors and the range of predictions with the different values of the R parameter at $N^4\text{LO}$ remain small. This again can be compared with predictions for the nonlocal force [17] shown in [29]. The improved interaction leads at $E_\gamma=60.8$ MeV to a theoretical uncertainty approximately two times smaller than for the older force. The chiral predictions at the lower energy are in agreement with the data and are slightly above them at the higher energy. This may indicate that more sophisticated structures in the 2N current operator are required. The AV18 predictions are closer to the data but still overpredict them at the maximum of the photon asymmetry.

IV. RESULTS FOR NUCLEON-DEUTERON RADIATIVE CAPTURE

The three-nucleon systems pose another possibility to test models of nuclear dynamics. In Fig.6 we show the differential cross section for the neutron-deuteron radiative capture reaction at the neutron laboratory energy $E_n=9.0$ MeV (upper row), and for the proton-

deuteron radiative capture at the proton laboratory energies $E_p=29.0$ MeV (central row) and $E_p=95.0$ MeV (lower row). For the neutron capture process the chiral predictions at next-to-leading order (NLO) and N^2 LO agree with data but the N^3 LO or N^4 LO forces shift the predictions about 10% above the experimental points. It was shown in [31] that for the case of nonlocal regularization the 3N force reduces the cross section for this process at low energies also by about 10%. Thus it will be interesting to check if the same is true for the locally regularized 3N force. The width of the band representing the truncation errors at N^4 LO is small and the cross section is practically independent from the choice of the regulator value.

In the case of the proton-deuteron radiative capture at presented here proton energies the 3N force effects (shown in Fig. 5 of Ref. [31]) are different. At $E_p=29.0$ MeV they are small, so it is very likely that agreement of N^4 LO predictions with the data, observed in Fig.6, will remain, if the locally regularized 3N force is included. At $E_p=95$ MeV 3N force increases the cross section, so again it is possible that the observed underprediction of the cross section will be removed by the 3N interaction. It seems rather accidental that even at the highest energy the LO predictions are relatively close to the other ones. The truncation errors and cut-off dependence remain small for both proton energies. This is very different from results obtained with explicit chiral MEC at LO and dominant terms at NLO for the old version of the potential with nonlocal regularization which show strong cut-off dependence - around 50% at $E_p=50$ MeV (see Fig.4 of [29]). However, one has to be careful comparing predictions from Ref. [29] with the current ones since it is expected that part of the cut-off dependence seen in Ref. [29] should be absorbed into short-range currents, neglected in Ref. [29]. Nevertheless, much smaller cut-off dependence and truncation errors observed with the local force [21, 22] are very promising.

The size of the truncation errors clearly depends on the value of the regularization parameter R . In Fig. 7 we compare the truncation errors for the same differential cross section as shown in the last row of Fig.6, i.e. at $E_p=95$ MeV but for $R=0.8$ fm (left), $R=1.0$ fm (middle) and $R=1.2$ fm (right). In all cases the truncation errors decrease with the growing chiral order and are very small at N^4 LO for $R=0.8$ and 1.0 fm, and much bigger for $R=1.2$ fm. In particular, in the maximum of the cross section the bands width at N^4 LO are $0.003 \mu\text{b/sr}$ both for $R=0.8$ and 1.0 fm and $0.017 \mu\text{b/sr}$ for $R=1.2$ fm. The latter value is still approximately twice less than the spread of predictions at N^4 LO obtained with different values of regularization parameter, which amounts $\Delta=0.038 \mu\text{b/sr}$ in the maximum of the cross section. This shows, that fixing the value of regulator parameter is important for the analysis of theoretical uncertainties. In Refs. [21, 22] the values of regularization parameter $R=0.9$ fm and $R=1.0$ fm have been recommended due to the best description of the nucleon-nucleon scattering data. Our findings on truncation errors also support this choice.

As an example of a polarization observable we choose the deuteron vector analyzing power A_Y and show it in Fig. 8 at two deuteron laboratory energies $E_d=17.5$ MeV (top) and $E_d=95$ MeV (bottom). For both energies we observe nice behaviour at orders above N^2 LO - the convergence with respect to chiral order is very good and truncation errors are diminishing. Also the cut-off dependence is negligible. That is a significant improvement when compared to the case of the nonlocal regularization [31]. At both energies the data description is poor, however this observable depends strongly on the details of the nuclear current operator [34].

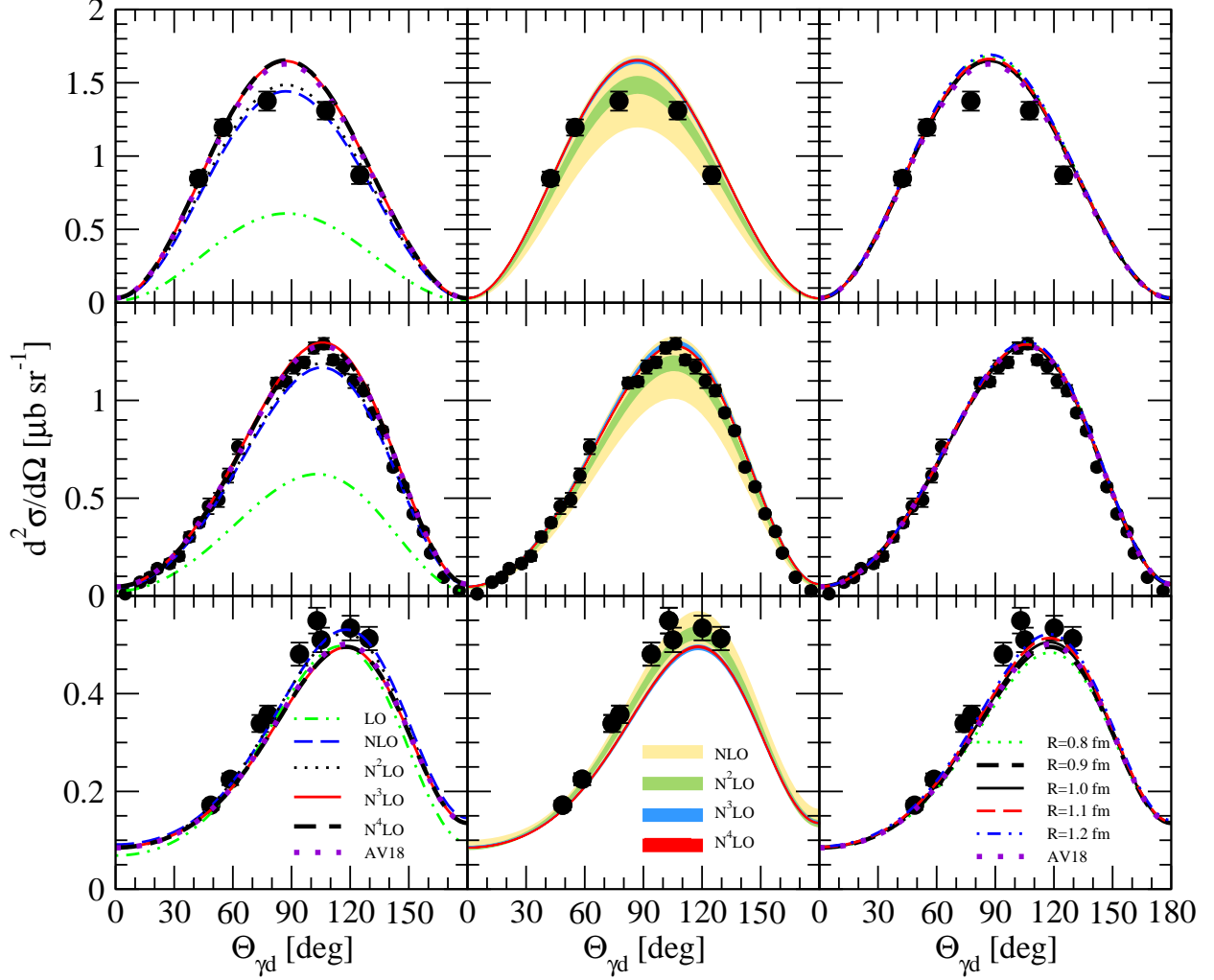


FIG. 6. (Color online) The differential cross section $d^2\sigma/d\Omega$ for the $n + d \rightarrow {}^3\text{H} + \gamma$ reaction at $E_n=9.0$ MeV (top) and for the $p + d \rightarrow {}^3\text{He} + \gamma$ reaction at $E_p=29$ MeV (middle) and $E_p=95$ MeV (bottom). The left column shows the convergence of predictions at $R=0.9$ fm with respect to the order of the chiral expansion (curves as in Fig. 2). The middle column shows the truncation errors (see text) at the different orders of the chiral expansion (bands as in Fig. 2). The right column shows the dependence of the predictions at N⁴LO on the value of the R parameter (curves as in Fig. 2). The data at $E_n=9.0$ MeV are from [59], at $E_p=29$ MeV from [60] and at $E_p=95$ MeV from [61].

V. THREE-BODY ${}^3\text{He}$ PHOTODISINTEGRATION

We choose the semi-inclusive cross section $\frac{d^3\sigma}{d\Omega_p dE_p}$ as an example of an observable for three-body ${}^3\text{He}$ photodisintegration. In this process only one of the three outgoing nucleons is detected and we assume that it is a proton. For this observables we have prepared three different Figs. 9-11, showing the dependence on the chiral order, error estimates and the dependence on the regulator value at N⁴LO. In all three figures we show the cross section at photon laboratory energy $E_\gamma = 40$ MeV and 120 MeV as a function of the final proton energy for the proton emerging at four angles Θ_p with respect to the photon beam:

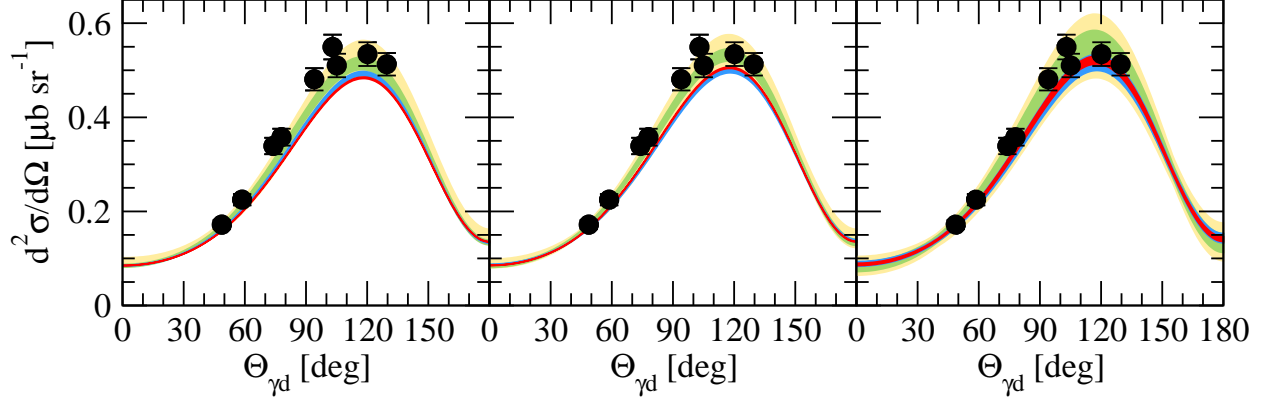


FIG. 7. (Color online) The truncation errors at different orders of the chiral expansion for the same cross section as shown in Fig.6 but at the proton energy $E_p=95$ MeV only. The predictions have been obtained using the value of the regularization parameter $R=0.8$ fm (left), $R=1.0$ fm (middle) and $R=1.2$ fm (right). Bands are as in Fig. 2 and data are from [61].

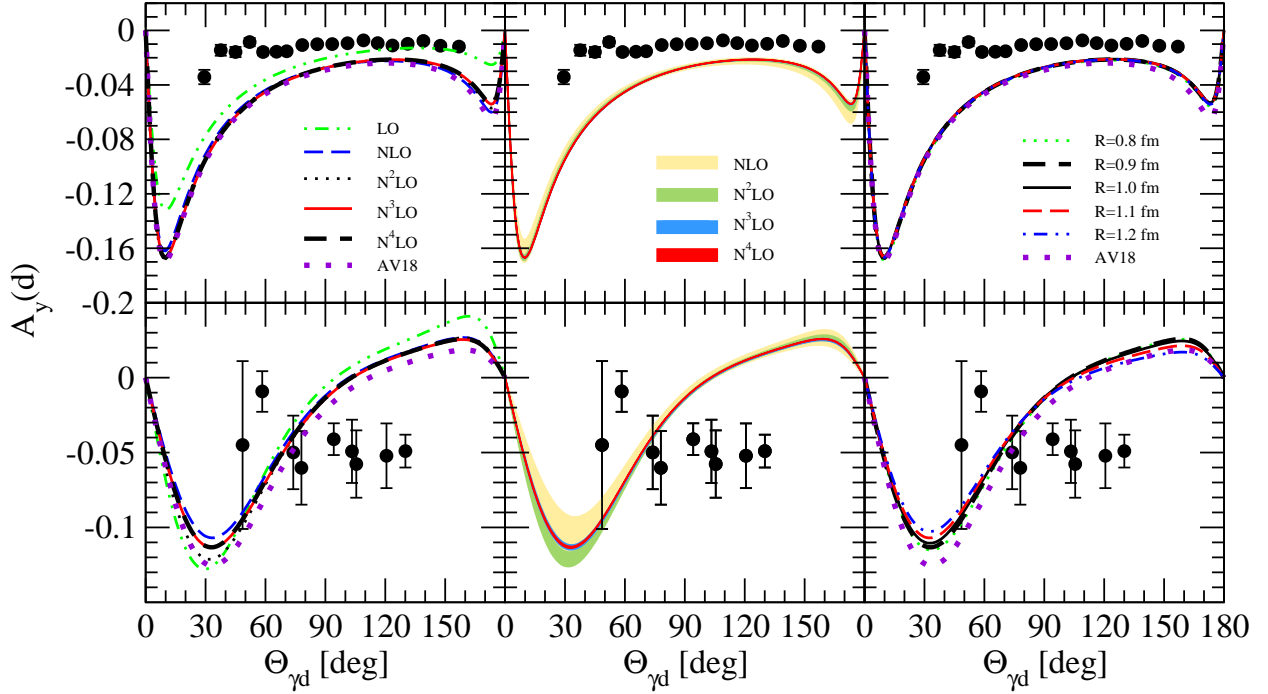


FIG. 8. (Color online) The deuteron analyzing power $A_y(d)$ for the $p + d \rightarrow {}^3\text{He} + \gamma$ reaction at the deuteron laboratory energies $E_d=17.5$ MeV (top) and $E_d=95$ MeV (bottom). The left column shows the convergence of the predictions at $R=0.9$ fm with respect to the order of the chiral expansion (curves as in Fig. 2). The middle column shows the truncation errors at the different orders of the chiral expansion (bands as in Fig. 2). The right column shows the dependence of predictions at $N^4\text{LO}$ on the value of the R parameter (curves as in Fig. 2). The data at $E_p=17.5$ MeV are from [62, 63] and at $E_p=95$ MeV from [61].

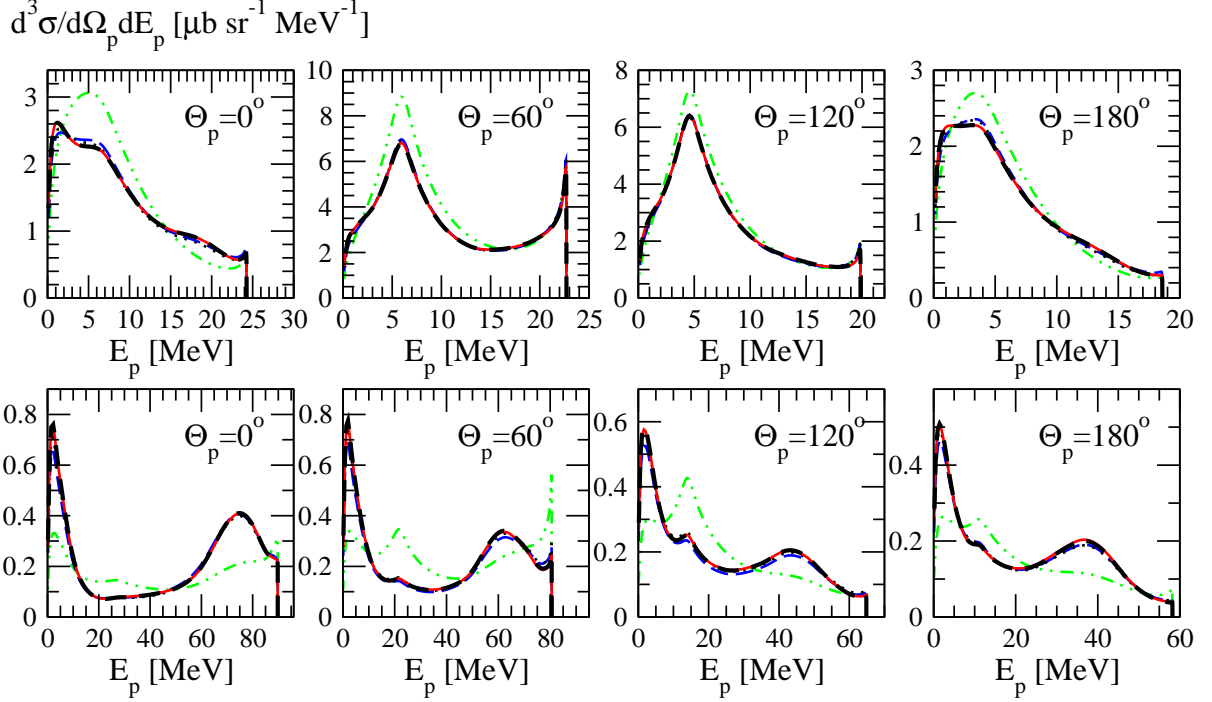


FIG. 9. (Color online) The semi-inclusive ${}^3\text{He}(\gamma, p)\text{pnpn}$ cross section $\frac{d^3\sigma}{d\Omega_p dE_p}$ at $E_\gamma=40$ MeV (top) and $E_\gamma=120$ MeV (bottom), as a function of the outgoing proton energy E_p for various angles Θ_p of the outgoing proton momentum with respect to the photon beam in the laboratory system. The predictions were obtained within the SNC+Sievert model and with the regulator $R = 0.9$ fm. The double-dotted-dashed green, dashed blue, dotted black, solid red and thick dashed black curves correspond to LO, NLO, N^2LO , N^3LO and N^4LO predictions, respectively.

$\Theta_p = 0^\circ, 60^\circ, 120^\circ$ and 180° . Since we focus here on predictions of the new local chiral potential, we refer the reader to Refs. [64] and [36] for the discussion on the origin of structures observed in the spectra.

In Fig. 9 we show the convergence of predictions with respect to the order of the chiral expansion for the detected proton at $E_\gamma = 40$ MeV (top) and $E_\gamma = 120$ MeV (bottom). Only predictions at LO are far away from the rest and are surely not sufficient to describe the data. The other predictions are close to each other and, in particular the N^3LO and N^4LO results, practically overlap.

The bands giving the truncation errors for the semi-inclusive cross section are shown in Fig. 10. At the photon laboratory energy $E_\gamma=40$ MeV a big contribution from higher orders is expected at the NLO (the yellow band) and still noticeable addition is expected at N^2LO (the green band). At higher orders bands are very narrow and they practically overlap. Thus one can conclude that for the presented here cross section, calculations at N^3LO should be sufficient. At the higher photon laboratory energy $E_\gamma=120$ MeV the magnitude of the truncation errors is sizable even at N^4LO .

Finally, in Fig.11 we explicitly show the dependence of the cross section on the value of the parameter R used to regularize the chiral forces at N^4LO . The cut-off dependence at $E_\gamma=40$ MeV is weak and its size is comparable with the truncation errors. At the higher energy clear differences between predictions based on different values of R are seen. The range of predictions due to the different values of R usually slightly exceeds the theoretical

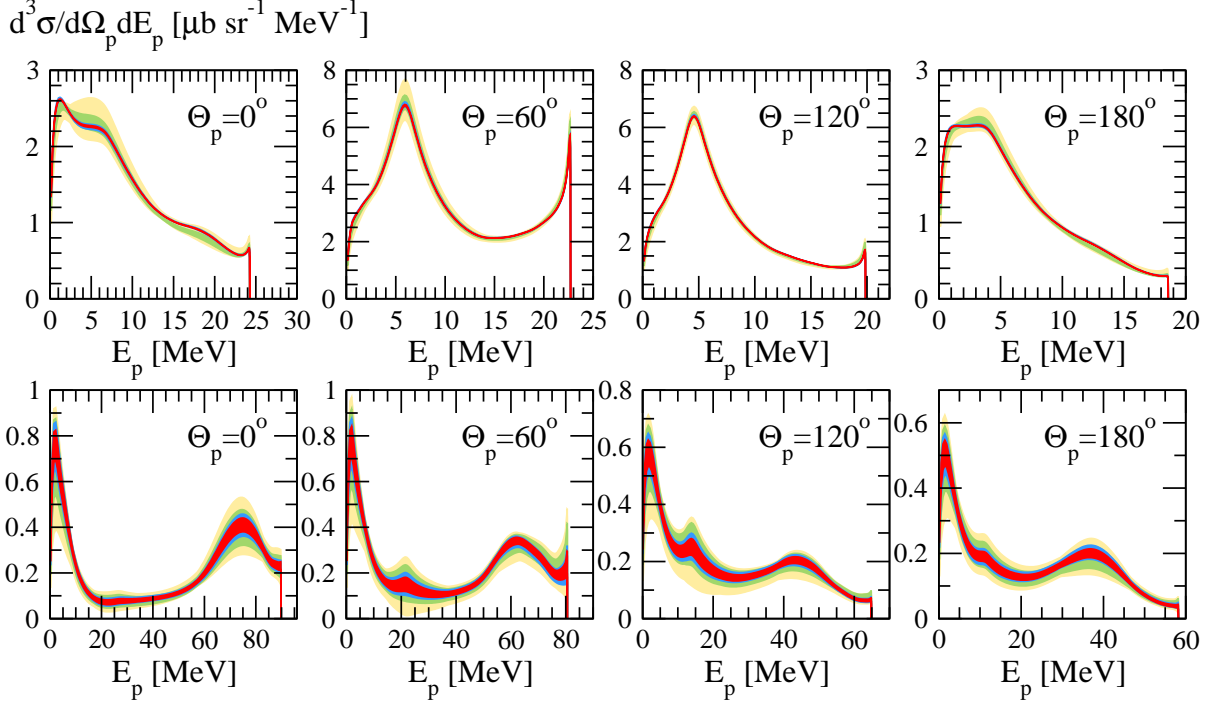


FIG. 10. (Color online) The estimated higher order truncation errors for the cross sections shown in Fig. 9. The yellow, green, turquoise and red bands show the theoretical uncertainties at NLO, N²LO, N³LO and N⁴LO, respectively.

uncertainties at N⁴LO shown in Fig. 10. Note, however, that the values $R=0.9$ fm and $R=1.0$ fm are preferred [21, 22].

VI. MUON CAPTURE

For the muonic deuterium atom the weak capture process leads to two neutrons and a muon neutrino in the final state. The total capture rates Γ_d for this process are given in Tab. I. We also give the truncation error $\delta(\Gamma_d)^{(i)}$ (Eq. 2.6) at a given order for $R=0.9$ fm (the next-to-last column) and the maximal difference between predictions with different value of the regulator R at a given order, Δ (the last column). We applied the SNC+RC model of the current operator and used values of the regularization parameter R in the range from 0.8 to 1.2 fm. The truncation errors decreases significantly with the increasing order of the chiral expansion, confirming nice convergence of capture rate. At N⁴LO and $R=0.9$ fm $\delta(\Gamma_d)^{(5)}$ is about 0.02%. The truncation errors for $R=1.2$ fm (not shown in the table) are much bigger, reaching 0.18% at N⁴LO. The cut-off dependence is also weak, at N⁴LO $\Delta=1.7$ s⁻¹ what amounts to about 0.44% of the capture rate at $R=0.9$ fm. The new predictions are also in agreement with the result based on the AV18 NN force, which for the same model of the weak current is 382.3 s⁻¹.

In the case of muon capture on ³He three different final states are possible. First, the capture process can lead to the non-breakup channel with the final ³H nucleus and the outgoing neutrino. Results concerning the total capture rate for this process are given in Tab. II. The LO predictions are far away from the other results, but starting from NLO we

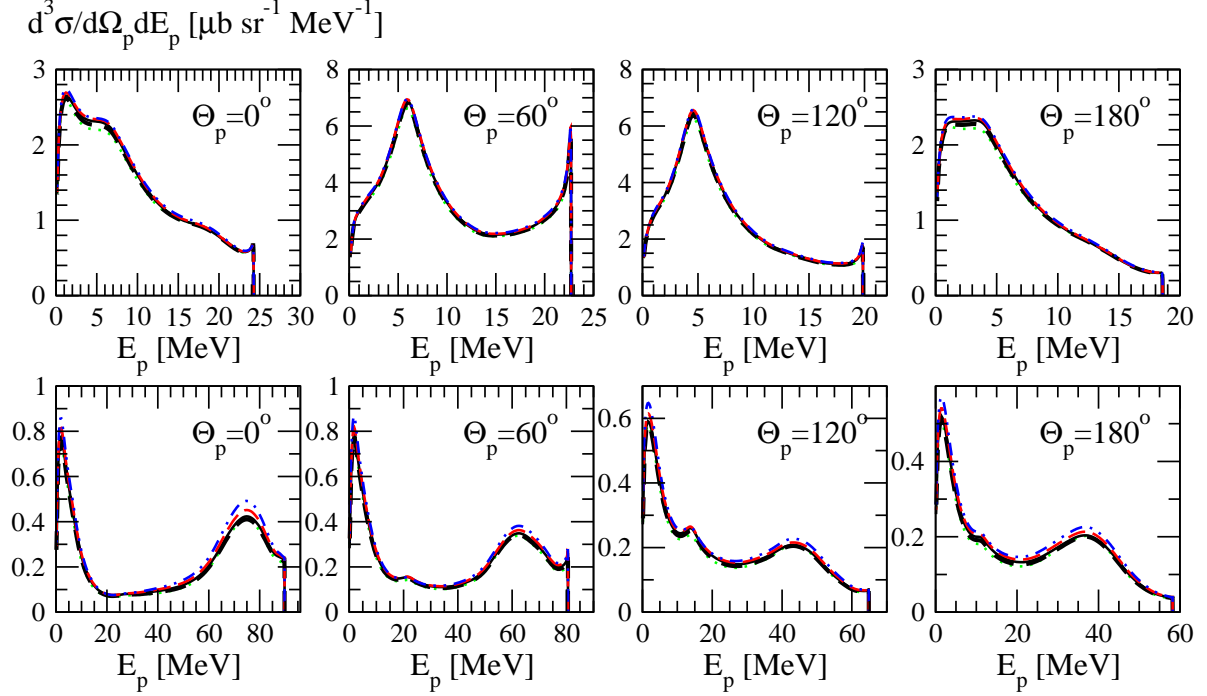


FIG. 11. (Color online) The cut-off dependence of the cross sections shown in Fig.9. The dotted green, thick dashed black, solid black, dashed red and double-dotted-dashed blue curves are for $R = 0.8, 0.9, 1.0, 1.1, 1.2$ fm, respectively.

see a nice convergence of results with respect to the order of the chiral expansion for all the values of R . The truncation error $\delta(\Gamma)^{(0)}$ at LO is over two orders of magnitude bigger than the one at N⁴LO. Its value at N⁴LO is approx. 0.07% (0.52%) of the capture rate using $R=0.9$ (1.2) fm. Also in this case the dependence on the cut-off parameter is very weak. The last column in Tab. II shows the maximal difference between predictions at a given order and for different regulators R , Δ , which at N⁴LO reaches approximately 1.76% for ³He - ³H transition. The capture rate obtained for this process with the AV18 NN potential and using the same model of weak current (SNC+RC) equals 1295 s⁻¹ and is very close to the chiral value.

For both above-mentioned processes we observe that the cut-off dependence dominates the truncation errors if all five considered here values of the regulator are taken into account in agreement with the arguments given in [44]. If one restricts oneself only to the suggested values of the regulator ($R=0.9$ fm or $R=1.0$ fm) then the truncation errors and the spread due to the different R are of the same order. We also find, for both capture processes, a small value of Δ at LO, which seems however to us somewhat accidental. It is also interesting to notice that the total capture rates reach their maxima at the same values of the regulator $R=0.9$ fm and 1.0 fm. Finally, we emphasize that the truncation error $\delta(\Gamma_d)$ at N²LO and higher orders, $\delta(\Gamma_d)^{(\geq 3)}$, estimated using Eq. (2.6) does not include information about the actual size of corrections $\Delta\Gamma_d^{(\geq 3)}$, which is not available from the incomplete calculations presented here. Also, the uncertainty from the truncation of the chiral expansion of the exchange current operators is not taken into account. Thus, the obtained values of $\delta(\Gamma_d)$ may underestimate the actual theoretical uncertainty at higher orders. In the future, more complete calculations will provide information on the size of contributions beyond N²LO

chiral order	$R=0.8$ fm	$R=0.9$ fm	$R=1.0$ fm	$R=1.1$ fm	$R=1.2$ fm	$\delta(\Gamma_d)$	Δ
LO	396.0	397.4	398.4	398.9	399.2	21.02	3.2
NLO	384.2	385.8	387.2	388.6	389.8	4.84	5.6
N ² LO	385.0	386.1	387.2	388.3	389.3	1.11	4.3
N ³ LO	386.8	386.4	385.2	384.3	383.2	0.26	3.6
N ⁴ LO	385.5	386.1	386.3	385.6	384.6	0.06	1.7

TABLE I. The doublet capture rates Γ_d in $[s^{-1}]$ for the $\mu^- + d \rightarrow n + n + \nu_\mu$ process obtained within the NN interaction at given order and the SNC+RC model of the nuclear weak current operator (see text). In the next-to-last column the truncation error $\delta(\Gamma_d)$ at given order of the chiral expansion for the doublet capture rate, obtained for $R=0.9$ fm, is given. In the last column the spread of the results at a given chiral order due to the different R values, Δ in $[s^{-1}]$, is shown.

chiral order	$R=0.8$ fm	$R=0.9$ fm	$R=1.0$ fm	$R=1.1$ fm	$R=1.2$ fm	$\delta(\Gamma)$	Δ
LO	1610	1618	1610	1594	1572	314.0	46
NLO	1330	1357	1381	1405	1427	72.2	97
N ² LO	1337	1356	1376	1395	1415	16.6	78
N ³ LO	1314	1304	1289	1278	1266	3.8	48
N ⁴ LO	1296	1307	1308	1299	1285	0.9	23

TABLE II. The total capture rates Γ in $[s^{-1}]$ for the $\mu^- + {}^3\text{He} \rightarrow {}^3\text{H} + \nu_\mu$ process obtained within the NN interaction at given order and the SNC+RC model of the nuclear weak current operator (see text). In the next-to-last column the truncation error $\delta(\Gamma)$ at i -th order of the chiral expansion for the total capture rate, obtained for $R=0.9$ fm, is given. In the last column the spread of the results at a given chiral order due to the different R values, Δ in $[s^{-1}]$, is shown.

which would allow us to perform a more reliable uncertainty quantification.

In Fig. 12 we show the differential capture rates for the $\mu^- + {}^3\text{He} \rightarrow d + n + \nu_\mu$ (top) and $\mu^- + {}^3\text{He} \rightarrow p + n + n + \nu_\mu$ (bottom) processes as a function of the outgoing neutrino energy E_ν . For both processes the convergence of differential capture rates at $R=0.9$ fm with respect to the chiral order looks similar. The NN force at LO underestimates the higher orders capture rates by a factor of approximately 3. The NLO and N²LO predictions are close to each other and finally the values at N³LO and N⁴LO are again very similar. The contributions from orders beyond LO play a significant role only above $E_\nu \approx 80$ MeV in both channels. As in the case of observables for electromagnetic processes presented in the

chiral order	$R=0.8$ fm	$R=0.9$ fm	$R=1.0$ fm	$R=1.1$ fm	$R=1.2$ fm	$\delta(\Gamma)$	Δ
LO	262	282	312	350	392	304.0	130
NLO	536	525	515	504	492	69.9	44
N ² LO	547	539	529	518	507	16.1	40
N ³ LO	584	586	592	596	603	3.7	19
N ⁴ LO	590	584	583	587	595	0.9	12

TABLE III. The same as in the Tab. II but for the $\mu^- + {}^3\text{He} \rightarrow d + n + \nu_\mu$ process.

chiral order	$R=0.8$ fm	$R=0.9$ fm	$R=1.0$ fm	$R=1.1$ fm	$R=1.2$ fm	$\delta(\Gamma)$	Δ
LO	95	99	105	113	120	70.0	26
NLO	159	157	154	151	148	16.1	11
N ² LO	161	159	157	154	151	3.7	10
N ³ LO	169	169	171	172	175	0.9	6
N ⁴ LO	170	169	169	170	173	0.2	4

TABLE IV. The same as in the Tab. II but for the $\mu^- + {}^3\text{He} \rightarrow \text{p} + \text{n} + \text{n} + \nu_\mu$ process.

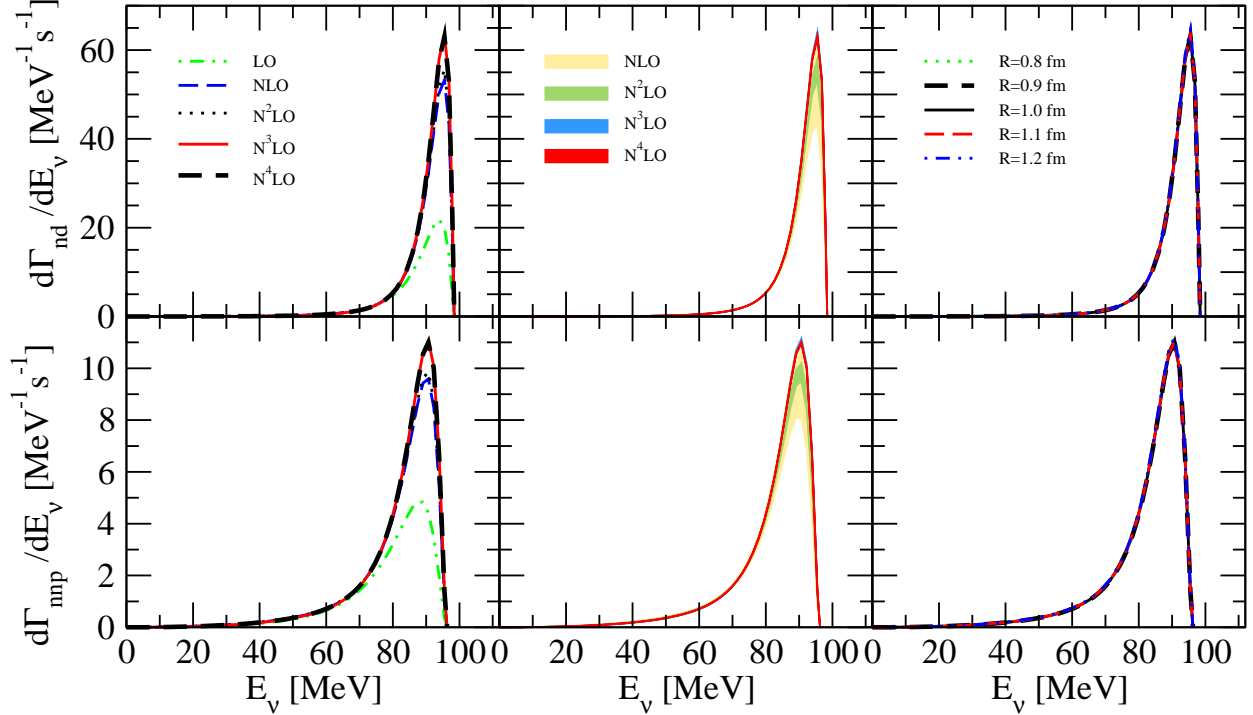


FIG. 12. (Color online) The differential capture rates for two- and three-nucleon breakup channels: $\frac{d\Gamma_{nd}}{dE_\nu}$ (top) and $\frac{d\Gamma_{nnp}}{dE_\nu}$ (bottom) as a function of the outgoing neutrino energy E_ν . The left column shows the convergence of predictions at $R=0.9$ fm with respect to the chiral expansion order (curves for chiral predictions only as in Fig. 2). The middle column shows the truncation errors at the different orders of the chiral expansion (bands as in Fig. 2). The right column shows the dependence of predictions at N⁴LO on the value of the R parameter (curves for chiral predictions only as in Fig. 2).

previous sections, the truncation errors are very small at the higher orders, pointing to a full convergence of nuclear forces with respect to the chiral expansion. The cut-off dependence is small and predictions for different regulators overlap, except for the region of the maximal capture rate values. However, even in this case the difference between predictions based on the different R values amounts only to 2.7% (2.3%) at $E_\nu=95.5$ (90.7) MeV for the two-body (three-body) channel.

The total capture rates for both breakup channels, given in Tabs. III and IV show similar behaviour as ones with the ${}^3\text{H}$ in the final state, given in Tab. II. Both measures of theoretical uncertainties, $\delta(\Gamma)$ and Δ , decreases with the chiral order, and are below 2.5% at N⁴LO.

Obtained here values of the capture rates are in agreement with corresponding results [33] for the AV18 force which are 604 s^{-1} and 169 s^{-1} for the $n+d$ and $n+n+p$ final states, respectively.

VII. SUMMARY

We applied the recently developed improved chiral NN forces with the semi-local regularization [21, 22] to a theoretical description of the deuteron and ^3He photodisintegration reactions as well as to the proton-deuteron radiative capture and the muon capture processes on the deuteron and ^3He . The single nucleon electromagnetic current supplemented by implicit many-body contributions included via the Siegert theorem was used for the processes with real photons. For the muon capture reactions the single nucleon weak current operator was used supplemented with the dominant, p^2/M_{nucl}^2 relativistic corrections. Despite their simplicity such models of nuclear currents are sufficient to realize the main goal of this work, which is to verify the usefulness of the locally regularized NN chiral forces in a description of electroweak processes at energies below the pion production threshold.

For all investigated reactions we could confirm the desired behavior of the used NN interaction. Namely, we observed fast convergence of the predictions with respect to the order of the chiral expansion - for all studied observables predictions at $N^4\text{LO}$ are very close to the ones at $N^3\text{LO}$. We also observe very weak dependence of our results on the value of the local regulator R . Especially, predictions with the recommended values of regulator [21, 22], $R=0.9 \text{ fm}$ and $R=1.0 \text{ fm}$, usually overlap at $N^4\text{LO}$. The observed cut-off dependence is much weaker than the one found in Ref. [31] for the older chiral forces [17], which were regularized directly in momentum space using nonlocal regulators. Finally, we estimate the truncation errors coming from neglecting higher order contributions. These theoretical uncertainties decrease with the chiral order and are very small beyond $N^2\text{LO}$, except for the highest energies studied here. The magnitude of the truncation errors depends on the value of the regulator R and is the biggest for $R=1.2 \text{ fm}$. The sizes of the truncation errors at $R=0.9 \text{ fm}$ and $R=1.0 \text{ fm}$ are comparable; they are of the same order as the difference between predictions obtained using these regulators. When all the R values are taken into account, the spread of predictions is usually bigger than the truncation error, even that for $R=1.2 \text{ fm}$. We conclude that in the future only recommended values $R=0.9 \text{ fm}$ and $R=1.0 \text{ fm}$ should be used. However, it would be interesting to confirm this observation in nuclear structure calculations.

The quality of the description of the data is rather satisfactory but leaves room for improvement by including contributions from 3N forces and many-body parts of the nuclear current operators. Thus, it will be important to identify observables which are sensitive to the details of the dynamical framework. One of the candidate is the deuteron analyzing power T_{22} in the deuteron photodisintegration process. Experimental efforts focused on precise and systematic measurements of such observables would be very important to provide a solid basis for a detailed study of chiral dynamics.

We may thus conclude that the present work confirms the importance of the improved chiral NN potential with the local regularization for few-body investigations in a broad range of energies. Of course we are aware that the final conclusions about the observed patterns can be drawn only when consistent 3N force and current operators at all the considered orders of the chiral expansion are included, but the predictions presented here constitute a promising, inescapable first step in this direction.

ACKNOWLEDGMENTS

Authors would like to thanks the members of the LENPIC collaboration for discussions. This work was supported by the Polish National Science Center under Grants No. DEC-2013/10/M/ST2/00420. and DEC-2013/11/N/ST2/03733, the ERC Starting Grant 259216 NuclearEFT, the DFG grant SFB/TR 16 "Subnuclear Structure of Matter" and by the Chinese Academy of Science (CAS) President's International Fellowship Initiative (PIFI) (Grant No. 2015VMA076). The numerical calculations have been performed on the supercomputer cluster of the JSC, Jülich, Germany.

-
- [1] J. Carlson and R. Schiavilla, *Rev. Mod. Phys.* **70**, 743 (1998).
 - [2] S. Bacca and S. Pastore, *J. Phys. G: Nucl. Part. Phys.* **41**, 123002 (2014).
 - [3] P. Kammel and K. Kubodera, *Annu. Rev. Nucl. Part. Sci.* **60**, 327 (2010).
 - [4] V.D. Efros, W. Leidemann, G. Orlandini, and N. Barnea, *J. Phys. G: Nucl. Part. Phys.* **34**, R459 (2007).
 - [5] L.E. Marcucci, M. Piarulli, M. Viviani, L. Girlanda, A. Kievsky, S. Rosati, and R. Schiavilla, *Phys. Rev.* **C83**, 014002 (2011).
 - [6] L.E. Marcucci, A. Kievsky, S. Rosati, R. Schiavilla, and M. Viviani, *Phys. Rev. Lett.* **108**, 052502 (2012).
 - [7] R. Machleidt and D.R. Entem, *Phys. Rept.* **503**, 1 (2011).
 - [8] E. Epelbaum, H.-W. Hammer, and Ulf-G. Meißner, *Rev. Mod. Phys.* **81**, 1773 (2009).
 - [9] E. Epelbaum, A. Nogga, W. Glöckle, H. Kamada, Ulf-G. Meißner, and H. Witała, *Phys. Rev.* **C66**, 064001 (2002).
 - [10] E. Epelbaum, A. Nogga, W. Glöckle, H. Kamada, Ulf-G. Meißner, and H. Witała, *Eur. Phys. J.* **A15**, 543 (2002).
 - [11] E. Epelbaum, A. Nogga, H. Witała, H. Kamada, W. Glöckle, and Ulf-G. Meißner, *Eur. Phys. J.* **A17**, 415 (2003).
 - [12] W. Glöckle, E. Epelbaum, H. Kamada, Ulf-G. Meißner, A. Nogga, and H. Witała, *Eur. Phys. J.* **A19**, 159 (2004).
 - [13] A. Kievsky, M. Viviani, L. Girlanda, and L.E. Marcucci, *Phys. Rev.* **C81**, 044003 (2010).
 - [14] M. Viviani, A. Baroni, L. Girlanda, A. Kievsky, L.E. Marcucci, and R. Schiavilla, *Phys. Rev.* **C89**, 064004 (2014).
 - [15] J. Carlson, S. Gandolfi, F. Pederiva, S.C. Pieper, R. Schiavilla, K.E. Schmidt, and R.B. Wiringa, *Rev. Mod. Phys.* **87**, 1067 (2015) *and references therein*.
 - [16] K. Hebeler, J.D. Holt, J. Menéndez, and A. Schwenk, *Ann.Rev.Nucl.Part.Sci.* **65**, 457 (2015).
 - [17] E. Epelbaum, W. Glöckle, and Ulf-G. Meißner, *Nucl. Phys.* **A747**, 362 (2005).
 - [18] H. Witała, J. Golak, R. Skibiński, and K. Topolnicki, *J. Phys. G: Nucl. Part. Phys.* **41**, 094011 (2014).
 - [19] J. Golak *et al.*, *Eur. Phys. J.* **A50**, 177 (2014).
 - [20] R. Skibiński, J. Golak, K. Topolnicki, H. Witała, E. Epelbaum, W. Glöckle, H. Krebs, A. Nogga, and H. Kamada, *Phys. Rev.* **C84**, 054005 (2011).
 - [21] E. Epelbaum, H. Krebs, and Ulf-G. Meißner, *Eur. Phys. J.* **A51**, 53 (2015).
 - [22] E. Epelbaum, H. Krebs, and Ulf-G. Meißner, *Phys. Rev. Lett.* **115**, 122301 (2015).
 - [23] S. Binder *et al.*, *Phys. Rev.* **C93**, 044002 (2016).

- [24] T.-S. Park, D.-P. Min, and M. Rho, Nucl. Phys. **A596**, 515 (1996).
- [25] S. Pastore, R. Schiavilla, and J.L. Goity, Phys. Rev. **C78**, 064002 (2008).
- [26] A. Baroni, L. Girlanda, S. Pastore, R. Schiavilla, and M. Viviani Phys. Rev. **C93**, 015501 (2016).
- [27] S. Kölling, E. Epelbaum, H. Krebs, and Ulf-G. Meißner, Phys. Rev. **C80**, 045502 (2009).
- [28] S. Kölling, E. Epelbaum, H. Krebs, and Ulf-G. Meißner, Phys. Rev. **C84**, 054008 (2011).
- [29] D. Rospędzik, J. Golak, S. Kölling, E. Epelbaum, R. Skibiński, H. Witała, and H. Krebs, Phys. Rev. **C83**, 064004 (2011).
- [30] R. Skibiński, J. Golak, D. Rospędzik, K. Topolnicki, and H. Witała, Acta Phys. Polon. **B46**, 159 (2015).
- [31] R. Skibiński, J. Golak, H. Witała, W. Glöckle, A. Nogga, and E. Epelbaum, Acta Phys. Polon. **B37**, 2905 (2006).
- [32] G. Shen, L.E. Marcucci, J. Carlson, S. Gandolfi, and R. Schiavilla, Phys. Rev. **C86**, 035503 (2012).
- [33] J. Golak, R. Skibiński, H. Witała, K. Topolnicki, A.E. Elmenshneb, H. Kamada, A. Nogga, and L.E. Marcucci, Phys. Rev. **C90**, 024001 (2014).
- [34] J. Golak, H. Kamada, H. Witała H, W. Glöckle, J. Kuroś-Żołnierczuk, R. Skibiński, V.V. Kotlyar, K. Sagara, and H. Akiyoshi, Phys. Rev. **C62**, 054005 (2000).
- [35] R. Skibiński, J. Golak, H. Kamada, H. Witała, W. Glöckle, and A. Nogga, Phys. Rev. **C67**, 054001 (2003).
- [36] J. Golak, R. Skibiński, H. Witała, W. Glöckle, A. Nogga, and H. Kamada, Phys. Rept. **415**, 89 (2005).
- [37] R. Skibiński, J. Golak, H. Witała, W. Glöckle, and A. Nogga, Eur. Phys. J. **A24**, 31 (2005).
- [38] H. Arenhövel, Z. Phys. A – Atoms and Nuclei **302**, 25 (1981).
- [39] H. Arenhövel, Lecture Notes in Physics, Vol. **426**, 1 (1994).
- [40] H. Arenhövel and M. Sanzone, Few-Body Syst. Suppl. **3**, 1 (1991).
- [41] J.D. Walecka, *Theoretical Nuclear and Subnuclear Physics* (Oxford University Press, New York, 1995).
- [42] W. Glöckle, H. Witała, D. Hüber, H. Kamada, and J. Golak, Phys. Rept. **274**, 107 (1996).
- [43] A. Nogga, D. Hüber, H. Kamada, and W. Glöckle, Phys. Lett. **B409**, 19 (1997).
- [44] E. Epelbaum *et al.*, in preparation.
- [45] R.B. Wiringa, V.G.J. Stoks, and R. Schiavilla, Phys. Rev. **C51**, 38 (1995).
- [46] R. Moreh, T.J. Kennett, and W.V. Prestwich, Phys. Rev. **C39**, 1247 (1989).
- [47] D.M. Skopik, Y.M. Shin, M.C. Phenneger, and J.J. Murphy, Phys. Rev. **C9**, 531 (1974).
- [48] M. Bosman, A. Bol, J.F. Gilot, P. Leleux, P. Lipnik, and P. Macq, Phys. Lett. **B82**, 212 (1979).
- [49] Y. Birenbaum, S. Kahane, and R. Moreh, Phys. Rev. **C32**, 1825 (1985).
- [50] R. Bernabei *et al.*, Phys. Rev. Lett. **57**, 1542 (1986).
- [51] S. Ying, E.M. Henley, and G.A. Miller, Phys. Rev. **C38**, 1584 (1988) *and references therein*.
- [52] I.A. Rachek *et al.*, Phys. Rev. Lett. **98**, 182303 (2007).
- [53] S.I. Mishnev *et al.*, Phys. Lett. **B302**, 23 (1993).
- [54] F. Ritz, H. Arenhövel, and T. Wilbois, Few-Body Syst. **24**, 123 (1998).
- [55] W. Tornow, N.G. Czakon, C.R. Howell, A. Hutcheson, J.H. Kelley, V.N. Litvinenko, S.F. Mikhailov, I.V. Pinayev, G.J. Weisel, and H. Witała, Phys. Lett **B574**, 8 (2003).
- [56] M.P. De Pascale *et al.*, Phys. Rev. **C32**, 1830 (1985).

- [57] I.E. Vnukov *et al.*, Pisma Zh. Eksp. Teor. Fiz. **43**, 510 (1986) [Sov. Phys. JETP Lett. 43, 659 (1986)].
- [58] V.P. Barannik *et al.*, Sov. J. Nucl. Phys. **38**, 667 (1983).
- [59] G. Mitev, P. Colby, N.R. Roberson, H.R. Weller, and D.R. Tilley, Phys. Rev. **C34**, 389 (1986).
- [60] B.D. Belt, C.R. Bingham, M.L. Halbert, and A. van der Woude, Phys. Rev. Lett. **24**, 1120 (1970).
- [61] W.K. Pitts *et al.*, Phys. Rev. **C37**, 1 (1988).
- [62] K. Sagara, H. Kiyoshi, S. Ueno, N. Nishimori, A. Motoshima, R. Koyasako, K. Nakashima, T. Fujita, K. Maeda, H. Nakamura, and T. Nakashima, AIP Conf. Proc. **334**, 467 (1995).
- [63] H. Akiyoshi, Ph.D. thesis, Kyushu University, 1997.
- [64] R. Skibiński, J. Golak, H. Witała, W. Glöckle, H. Kamada, and A. Nogga, Phys. Rev. **C67**, 054002 (2003).